JOURNAL OF SOLID STATE CHEMISTRY 118, 163–169 (1995)

Vibrational Spectroscopy of the C-Form of Yttrium Sesquioxide

Y. Repelin,* C. Proust,† E. Husson,†,[1] and J. M. Beny‡

*Laboratoire de Chimie Physique du Solide, URA CNRS 453, Ecole Centrale de Paris, 92295 Chatenay-Malabry Cedex, France; †Laboratoire de Physique et Mécanique des Matériaux, ESEM, Université d'Orléans et CRPHT-CNRS, 45071 Orléans Cedex 2, France; and ‡CRSCM-CNRS, 45071 Orléans Cedex 2, France

Received October 3, 1994; in revised form February 3, 1995; accepted February 6, 1995

Infrared and Raman spectra of polycrystalline Y_2O_3 as well as polarized Raman spectra of Y_2O_3 single crystals have been measured. A complete assignment of the bands is proposed. A normal coordinate analysis using a generalized valence force field enabled us to fit the observed frequencies with a satisfactory accuracy (3.5%). The calculated force constants are discussed and compared with those of α-Al_2O_3 exhibiting the same atomic coordination.

INTRODUCTION

Yttrium sesquioxide crystallizes in bixbyite structure as do many oxides including the sesquioxides of rare earth elements (1). The structure was studied by different authors using X-ray diffraction (2, 3) and neutron diffraction (4, 5). The most recent study is that of O'Connor and Valentine (5) and their data have been kept in the present work. The Raman and IR spectra of different rare earth sesquioxides have been published and for Y_2O_3, the Raman and IR frequencies are not unambiguously known. IR studies were made by Baun and McDevitt (6, 7) Nigara (8), and White and Keramidas (9). Raman scattering data were given by Schaack and Koningstein (10) working with single crystals of Y_2O_3 doped with 0.1% Er and 8% Eu and by Gouteron *et al.* (11) who studied single crystals of cubic sesquioxydes of Yb, Ho, Y, and Sc. They assigned their spectra with reference to the assignment proposed by Lejus and Michel (12) for a single crystal of isostructural oxide Er_2O_3. These works did not allow the observation of the expected number of frequencies. Moreover, no polarized Raman spectra of pure Y_2O_3 have been published yet.

First, we have completed these experimental data, then a normal coordinate analysis (NCA) has been carried out in order to obtain information about the chemical bonds from the calculated force constants.

[1] To whom correspondence should be addressed.

EXPERIMENTAL

Sintered pellets were prepared from high-purity (99.999%) Y_2O_3 powder by isostatic heating in air at 2120 K for 1 hr. A single crystal of Y_2O_3 was synthesized by the Verneuil method. It is very difficult to obtain single crystals of good optical quality, because the powder is fused at high temperature (melting point, 2680 K) and during cooling the crystal is subject to important internal stress; moreover, a phase transition occurs from the high-temperature hexagonal form to the cubic form and induces defects such as cleavage planes corresponding to the (111) planes of the cubic crystal. The single crystal was oriented by the Laue method in the (100) plane then cut in the form of a small cube with a 5-mm edge, and optically polished with a diamond paste.

The Raman and IR spectra of polycrystalline samples were recorded with a Brucker IFS 113 + 88 spectrometer equipped with a FRA 106 FT Raman accessory with a YAG excitation source (λ = 1.06 μm); for the Raman spectra, the scattered radiation was collected with a retrodiffusion geometry. The low-temperature spectra were recorded with a MMR Technology microcryostat with the Joule-Thomson gas expansion technique; a small Y_2O_3 crystal was fixed by grease to the sample holder. The IR absorption spectra were recorded in the range 4000–200 cm^{-1}: the samples were in the form of powder dispersed in CsI pellets. The IR reflectance spectra were obtained with a sintered Y_2O_3 platelet.

For the polarized Raman spectra of the crystal, a Dilor microprobe apparatus was used with 90° and 180° geometries and an argon ion laser was used as an excitation source (λ = 5145 Å). The normal coordinate analysis (NCA) treatment was carried out with the Schachtschneider GMAT and VSEC programs (13) modified by Bates (14) according to the Shimanouchi method (see Ref. 15), and a generalized valence force field (GVFF) was chosen.

0022-4596/95 $12.00

RESULTS AND DISCUSSION

Previous Structural Data

Yttrium sesquioxide crystallizes in the cubic system, space group $Ia3$ (T_h^7) with $a = 10.604$ Å and $Z = 16$. The structure is related to the fluorite structure, with each yttrium ion located at the center of a cube from which two of the eight nearest neighbor oxygens of the fluorite structure have been removed. The remaining oxygens are slightly displaced from the cube corners. Two arrangements of oxygens occur (Fig. 1): in the first, the oxygens are removed from a face diagonal and the yttrium ion is displaced from the center of the cube so that it has C_2 site symmetry; in the second, two oxygens are removed from the body diagonal producing a C_{3i} point symmetry at the yttrium ion site; the cubic cell contains 24 Y on C_2 (24*d*) sites and 8 Y on C_{3i} (8*b*) sites. Each Y atom in the C_{3i} site is bonded to oxygen atoms by six equivalent Y–O bonds of 2.28 Å (d_1 set); each Y atom in the C_{2i} site is bonded to two oxygens at 2.243 Å (d_2 set), two others at 2.274 Å (d_3 set), and two others are 2.233 Å (d_4 set). In this structure, each Y atom occupies a distorted octahedral site. YO_6 octrahedra are linked by corners and edges so that all O atoms (48*e*) are equivalent and are bonded to 4 Y atoms. The projection of the structure in the *ab* plane is given in Fig. 2.

A precise examination of the crystal framework shows that:

(i) A $Y_{(C_{3i})}O_6$ octahedron is linked by corners to six $Y_{(C_2)}O_6$ octahedra with $Y_{(C_{3i})}$–$Y_{(C_2)}$ distances of about 4.0 Å and by edges to six $Y_{(C_2)}O_6$ octahedra with $Y_{(C_{3i})}$–$Y_{(C_2)}$ distances of about 3.5 Å.

(ii) A $Y_{(C_2)}O_6$ octahedron is linked by corners to two other $Y_{(C_{3i})}O_6$ octahedra and four $Y_{(C_2)}O_6$ octahedra with $Y_{(C_2)}$–$Y_{(C_{3i})}$ and $Y_{(C_2)}$–$Y_{(C_2)}$) distances of about 4.0 Å and by edges to six $Y_{(C_2)}O_6$ octahedra with $Y_{(C_2)}$–$Y_{(C_2)}$ distances of about 3.5 Å.

The chemical environment of each set of bonds is the following:

(i) In a $Y_{(C_{3i})}O_6$ octahedron the d_1 bonds share their oxygen atom with another YO_6 octahedron linked to the first one by a corner and with two other YO_6 octahedra linked by an edge.

(ii) In a $Y_{(C_2)}O_6$ octahedron, the d_2 bonds share their oxygen atom with two other YO_6 octahedra linked to the first one by a corner and with another YO_6 octahedron linked by an edge.

(iii) The d_3 bonds share their oxygen atom with another YO_6 octahedron linked to the first one by a corner and with two other YO_6 linked by an edge.

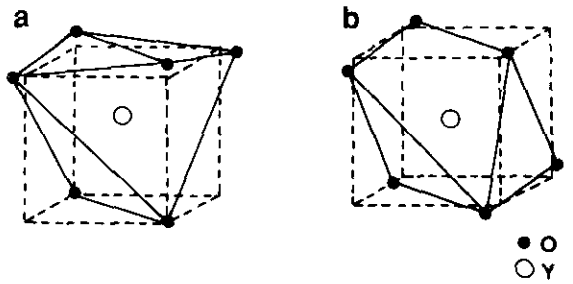

FIG. 1. Yttrium ion site in the cubic form of Y_2O_3. (a) C_2 site; (b) C_{3i} site.

(iv) The d_4 bonds share their oxygen atom with three other YO_6 octahedra linked to the first one by an edge.

Spectroscopic Data

As the structure is body-centered, the unit cell contains the primitive cell twice; the latter cell containing eight formula units was used for the theoretical numbering of vibrations. The irreducible representations for the optical and acoustical modes from the Bhagavantam method (16) are

$$\Gamma_{op} = \underbrace{4\,A_g}_{(R)} + \underbrace{4\,E_g}_{(R)} + \underbrace{14\,F_g}_{(R)} + \underbrace{5\,A_{2u}}_{(i)} + \underbrace{5\,E_u}_{(i)} + \underbrace{16\,F_u}_{(ir)}$$

$$\Gamma_{ac} = F_u,$$

where (R) stands for Raman active, (ir) for infrared active, and (i) for inactive. Twenty-two Raman lines of A_g, E_g, and F_g modes and 16 F_u infrared bonds are then predicted.

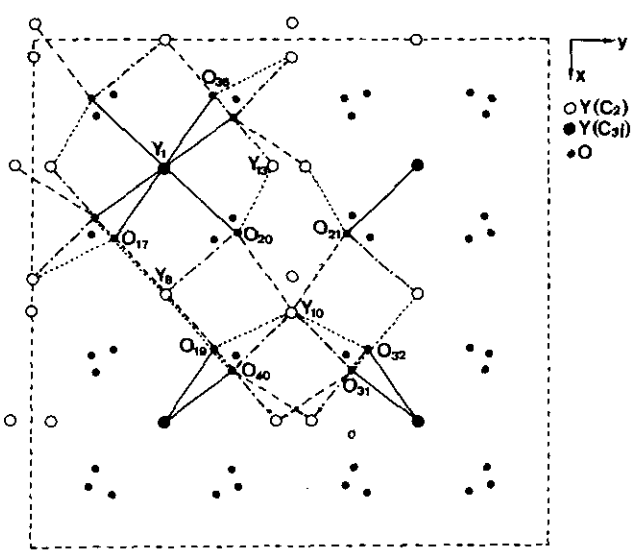

FIG. 2. Projection of the structure of Y_2O_3 in the *ab* plane. (d_1—d_2– – –d_3. . .d_4–·–· bonds).

Figure 3 displays the Raman spectrum of polycrystalline Y_2O_3 recorded at 300 K. Fourteen lines are observed instead of the 22 expected. The Raman spectrum recorded at 80 K is depicted in Fig. 4. The comparison of nitrogen and room temperature data reveals (i) a very small shift in frequency with temperature (about 2 cm^{-1}); (ii) a decrease in the linewidth with temperature for all the lines, allowing the 399 cm^{-1} line to be clearly separated from the 376 cm^{-1} line, but no new line appears. The broad range frequencies at 280–240 cm^{-1}, which were not assigned in the previous works, were not considered as fundamental lines in the present study.

Figure 5 displays some of the recorded polarized Raman spectra. Taking into account the orientation of the crystal we were able to separate the F_g modes from the $E_g + A_g$ modes, but it was not possible to separate the E_g modes from the A_g modes (see Table 1). These results complete those of Lejus and Michel (12), Gouteron *et al.* (11), and Schaak and Koningstein (10), who studied crystals oriented in the (111) plane; in this case, for the different polarizations, no mode may be separated from the two others but the calculated relative intensities of the lines theoretically permit the separation of those belonging to the three active modes. The examination of our spectra allows the characterization of the quality of the polarization: For example, the 318/329 cm^{-1} lines are quite well polarized. In the (zz) orientation the 318 cm^{-1} line is practically extinct; thus the 329 cm^{-1} line was assigned to an A_g or an E_g mode. In the (xz) orientations both lines are clearly present; thus these two lines were assigned to F_g modes. It seems that the optical quality of the crystal is sufficient to observe valuable polarizations of the lines. The Raman spectra $y(xz)y$ and $y(xz)x$ exhibit 13 lines instead of the 14 F_g expected. They were all assigned to F_g modes. In comparison to the previous assignments, we have the same frequencies as Schaak and Gouteron with additional lines at 564, 526, 329, and 193 cm^{-1}. The Raman spectra $y(zz)y$ and $y(zz)x$ exhibit 9 lines for the 4 A_g and 4 E_g expected lines. Lejus and Michel (12) and Gouteron *et al.* (11) assigned only one A_g mode at 161 cm^{-1} and 3 E_g modes for the 564, 376, and 193 cm^{-1} lines. The assignment proposed by Schaak and Koningstein is quite different with two A_g modes for the 376 and 161 cm^{-1} lines and two E_g modes for the 329 and 318 cm^{-1} lines. We have assigned the 161 cm^{-1} line to A_g mode and the 564 and 329 cm^{-1} lines to E_g modes in agreement with these authors; for the other lines we have made an assignment taking into account the two following assumptions:

(i) generally A_g modes are the most intense in a Raman spectrum,

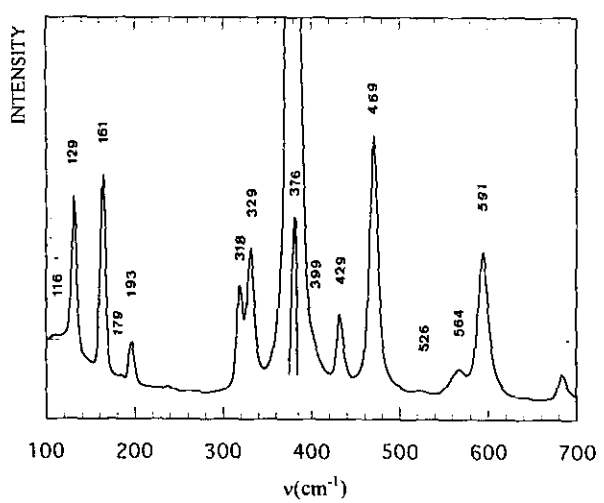

FIG. 3. Raman spectrum of Y_2O_3 at 300 K (obtained by the addition of 20,000 scans).

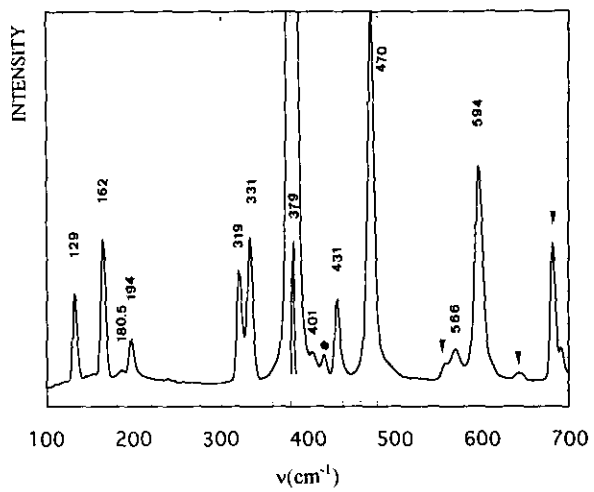

FIG. 4. Raman spectrum of Y_2O_3 at 80 K (obtained by the addition of 1000 scans). (●) grease lines; (▼) electronic Raman lines.

TABLE 1
Scattering Efficiency for a T_h Crystal with Various Incident and Observed Polarization Directions

	90° Geometry			
	HH	HV	VV	VH
	$y(xy)x$	$y(xz)x$	$y(zz)x$	$y(zy)x$
A_g			a^2	
E_g			$4b^2$	
F_g	d^2	d^2		d^2
	180° Geometry			
	HH	HV	VV	VH
	$y(xx)\bar{y}$	$y(xz)\bar{y}$	$y(zz)\bar{y}$	$y(zx)\bar{y}$
A_g	a^2		a^2	
E_g	$4b^2$		$4b^2$	
F_g		d^2		d^2

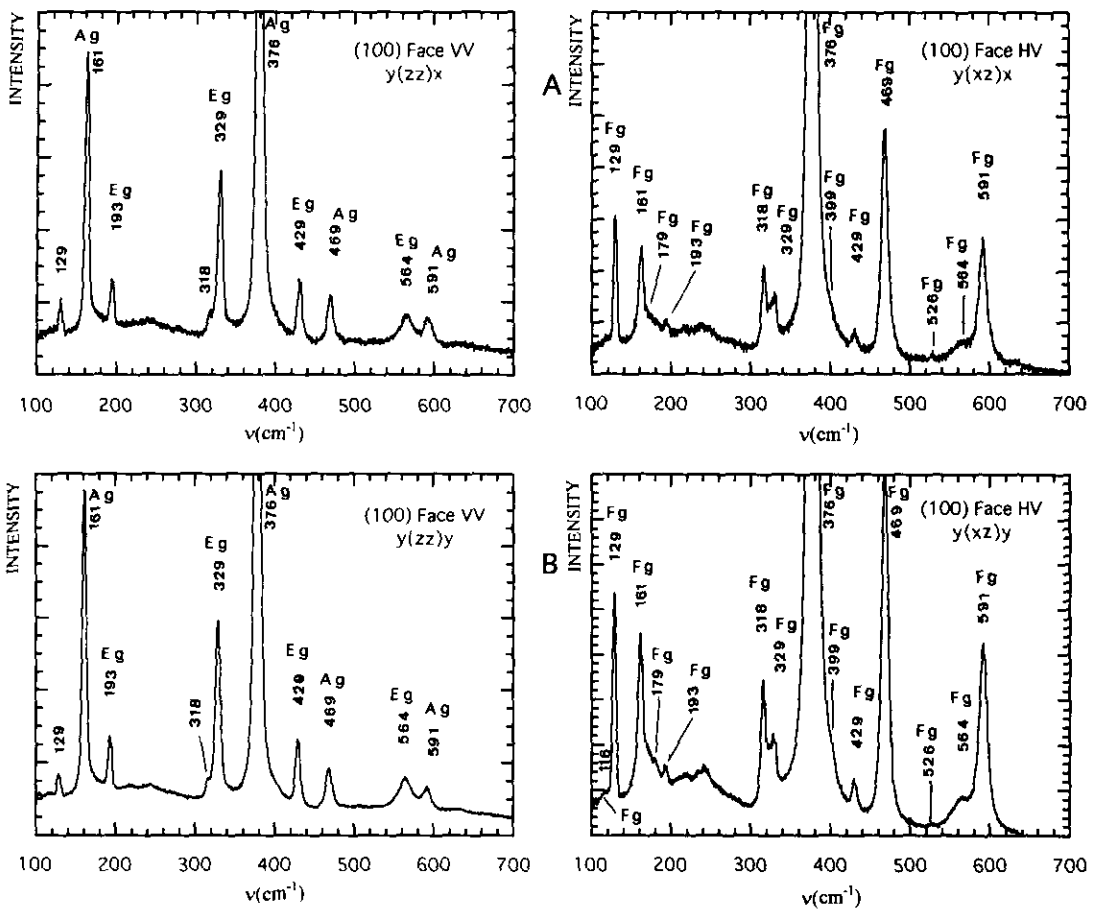

FIG. 5. Polarized Raman spectra of Y_2O_3. (The notation of Porto is used.)

(ii) one can observe that the lines seem to be grouped two by two in the (zz) spectra; in each group of two lines, there is surely one A_g mode and one E_g mode.

Thus we have assigned the 591 cm^{-1} frequency to the A_g mode (E_g mode at 564 cm^{-1}), the 376 cm^{-1} line to the A_g mode as Schaak did (E_g mode at 329 cm^{-1}), and the 193 cm^{-1} line to the E_g mode as Gouteron did (A_g line at 164 cm^{-1}). For the two remaining lines at 431 and 469 cm^{-1} which were only assigned to F_g modes in previous works, we have assigned the more intense line, at 469 cm^{-1}, to the A_g mode. The line at 129 cm^{-1} in the (zz) spectra was considered the residual F_g line.

The proposed assignment of the Raman frequencies is presented in Table 2 as are the previous assignments. It can be observed that all the A_g and E_g modes have the same value of frequency as an F_g mode, which explains why the number of observed lines in the spectra of Fig. 3 and 4 is less than the expected one.

Figure 6 displays the IR reflectance spectrum of a sintered platelet of Y_2O_3. We obtained the same features as Nigara (8) with additional Reststrahlen bands at 438 cm^{-1} and at the low frequencies of 238, 179, 168 and 120 cm^{-1}.

The IR absorption spectrum, given in Fig. 7, is again very close to that of Nigara's, but we did not clearly observe a band at 515 cm^{-1}, and the band at 562 cm^{-1} seems to exhibit a shoulder at about 580 cm^{-1}. In the calculations we have considered the TO values given by Nigara (see Table 5). The proposed assignment of the IR frequencies is presented in Table 3 as are the previous assignments.

Normal Coordinate Analysis

The internal coordinate sets introduced in the NCA are listed in Table 4. There are four sets of Y–O bond stretching: The d_1 set corresponds to the $Y_{(C_{3i})}$–O bonds, the d_2 to d_4 sets correspond to the three types of $Y_{(C_2)}$–O bonds. Seven sets of O–Y–O angle bending (γ) and four sets of Y–O–Y angle bending (α) were also considered. On the whole 384 internal coordinates were introduced.

In order to obtain a better fit between the observed and calculated frequencies, it was necessary to add interaction constants. Different stretching/stretching (d/d), stretching/bending (d/α, d/γ) and bending/bending (α/α, γ/γ, γ/α) interactions were introduced and only those

TABLE 2
Assignment of the Raman Spectrum of Cubic Y_2O_3

Schaak *et al.* (10)	White *et al.* (9)	Gouteron *et al.* (11)	Our results
597 F_g	603	592 F_g	591 $F_g + A_g$
	576	567 E_g	564 $F_g + E_g$
			526 F_g
473 F_g	480	468 F_g	469 $F_g + A_g$
434 F_g	440	430 F_g	429 $F_g + E_g$
		402 F_g	399 F_g
381 $F_g + A_g$	389	383 E_g	376 $F_g + A_g$
		379 F_g	
333 E_g	337	330 F_g	329 $F_g + E_g$
320 $F_g + E_g$	325	318 F_g	318 F_g
		194 E_g	193 $F_g + E_g$
		182 F_g	179 F_g
164 $F_g + A_g$	162	161 $F_g + A_g$	161 $F_g + A_g$
133 F_g		130 F_g	129 F_g
			116 F_g

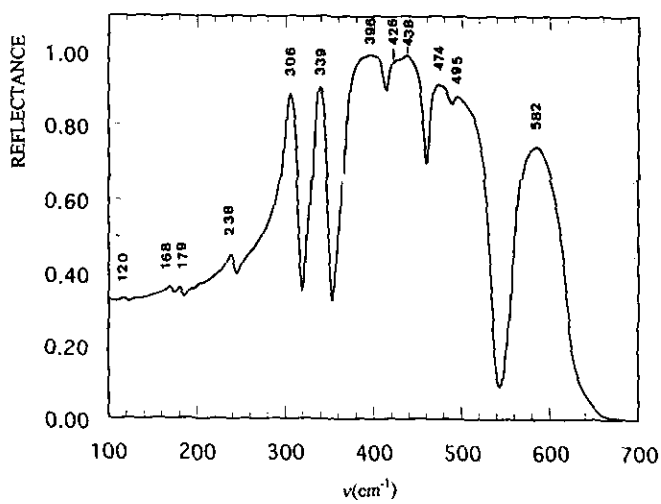

FIG. 6. IR reflectance spectrum of a sintered sample of Y_2O_3.

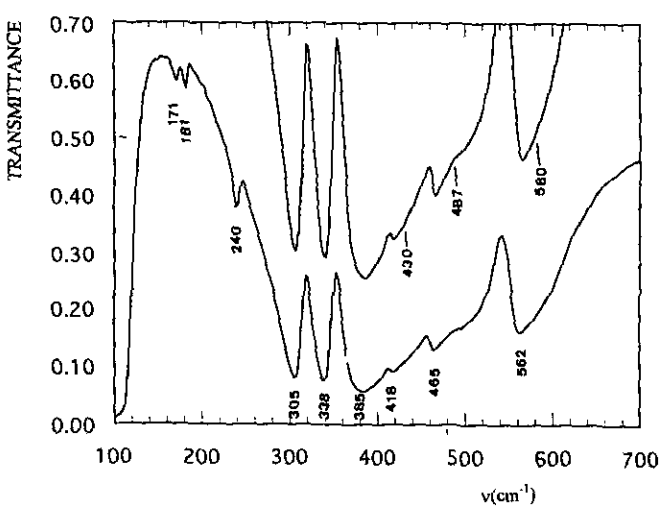

FIG. 7. IR transmittance spectrum of Y_2O_3.

TABLE 3
Assignment of the Infrared Spectra of Cubic Y_2O_3

Baun (6)	McDevitt (7)	White (9)	Nigara (8) R	Nigara (8) Ab	Our results R	Our results Ab
		570				580
561	561	562	585	561	582	562
500				515		
			495	490	495	487
	468	465	475	464	474	465
				445	438	430
	405	408	430	418	426	418
360	390	390	390	390	396	385
333	343	346	340	342	339	338
300	312	311	310	311	306	305
	242	243		242	238	242
	182	182		183	179	181
	171	171		172	168	171
	120	120		120	120	

Note. R, Reststrahlen bands; Ab, absorption bands.

TABLE 4
Definition and Calculated Force and Interaction Constants for Cubic Y_2O_3

	Definition	d(Å), α and γ(°)	f^a
d_1	Y_1O_{20}	2.28	1.20
d_2	$Y_{10}O_{20}$	2.24	1.25
d_3	$Y_{13}O_{20}$	2.27	0.80
d_4	Y_8O_{20}	2.33	0.90
γ_1	$O_{17}Y_1O_{20}$	99.67	0.42
γ_2	$O_{20}Y_1O_{36}$	79.50	0.42
γ_3	$O_{20}Y_{10}O_{21}$	88.03	0.47
γ_4	$O_{19}Y_{10}O_{20}$	100.20	0.47
γ_5	$O_{19}Y_{10}O_{31}$	78.80	0.47
γ_6	$O_{19}Y_{10}O_{40}$	79.11	0.42
γ_7	$O_{20}Y_{10}O_{40}$	79.40	0.42
α_1	$Y_1O_{20}Y_8$	98.88	0.20
α_2	$Y_1O_{20}Y_{13}$	100.66	
α_3	$Y_8O_{20}Y_{10}$	101.13	
α_4	$Y_8O_{20}Y_{13}$	100.23	
d_1/d_1	$O_{20}Y_1/Y_1O_{17}$		0.16
d_2/d_2	$O_{20}Y_{10}/Y_{10}O_{21}$		0.15
d_3/d_3	$O_{19}Y_{10}/Y_{10}O_{32}$		0.25
d_4/d_4	$O_{31}Y_{10}/Y_{10}O_{40}$		0.06
d_1/d_3	$Y_1O_{20}/O_{20}Y_{13}$		0.26
d_1/d_2	$Y_1O_{20}/O_{20}Y_{10}$		0.20
d_1/d_4	$Y_1O_{20}/O_{20}Y_8$		
d_2/d_3	$Y_{10}O_{20}/O_{20}Y_{13}$		0.10
d_2/d_4	$Y_{10}O_{20}/O_{20}Y_8$		
d_3/d_4	$Y_{13}O_{20}/O_{20}Y_8$		0.22

[a] Units: stretching and stretching/stretching in N · cm^{-1}, bending in N · cm · rad^{-2}.

having significant values were kept in the final refinement; all of these correspond to stretching/stretching interactions. They are listed in Table 4.

As already noted by Schaack and Koningstein (10) and Bloor and Dean (17), the vibrational spectra of Y_2O_3 exhibit two distinct frequency ranges; the frequencies above 300 cm^{-1} are practically identical for Y_2O_3 and isostructural rare earth cubic sesquioxides; thus, they are due to oxygen motions and deformations of YO_6 octahedra. The frequencies below 300 cm^{-1} vary in a ratio corresponding to the square root ratio of the atomic masses of *Ln* (*Ln* = rare earth) or Y atoms; thus, they are affected by the motions of rare earth or yttrium atoms in their octahedra.

On the basis of the internal coordinates, the highest frequencies may be assigned to Y–O bond stretching; as all oxygens exhibit the same coordination and as Y–O bonds have close lengths, it is not possible to predict if the vibration frequencies of the $Y_{(C_{3i})}O_6$ or those of the $Y_{(C_2)}O_6$ octahedra are the highest. As the YO_6 octahedra are linked by corners and edges leading to quite a compact structure, couplings surely occur. At lower frequencies, the O–Y–O bending modes and then the Y–O–Y bending modes are expected, with, again, many couplings.

In the first step of the calculations, identical force constants were fixed for the stretching of the four Y–O bonds as well as for the bending of all the O–Y–O angles and all the Y–O–Y angles. The examination of the potential energy distribution (PED) showed that the highest frequencies were due to coupled stretching modes of the d_1 and d_2 bonds. These two sets of bonds therefore have a force constant greater than the d_3 and d_4 constants for which the stretching modes appear at lower frequencies, coupled together or coupled with the d_1 and (or) d_2 stretching modes. We then refined separately the stretching force constants. All the O–Y–O angles are different; thus, their force constants have been also refined separately during the fit processing. In contrast, only one bending force constant was chosen for the four types of Y–O–Y angles which all have values close to 100°, and which do not have a great contribution in the PED. Only stretching/stretching interaction constants given in Table 4 have been kept, for all the others had very small values.

Table 5 presents the PED and the comparison between observed and calculated frequencies. The PED shows that an important number of frequencies are due to stretching modes; the O–Y–O and Y–O–Y bending modes are greatly coupled with the stretching modes. Only the lowest frequencies (<130 cm^{-1}) are pure bending modes. The comparison between observed and calculated frequencies reveals that a satisfactory fit (average error of about 3.5%) is obtained with 12 principal force constants and 8 interaction constants, i.e., 20 adjustable parameters for 27 observed frequencies. If only one value of force constant is kept for the 7 O–Y–O angle bending sets (average value of 0.44 $N \cdot cm \cdot rad^{-2}$), there are thus only 14 adjustable parameters and the average error between observed and calculated frequencies is 3.6%. Moreover, this force field could be transferred in the fits

TABLE 5
Comparison between Observed and Calculated Frequencies and Potential Energy Distribution (PED) in Cubic Y_2O_3

Mode	Obs.	Calc.	PED
Ag	591	582.9	$39d_1 + 44d_2 - 9d_{12}$
	469	483.4	$31d_1 + 10d_2 + 21d_3 + 17d_4 + 26\gamma - 9d_{13} + 8d_{34}$
	376	362.7	$7d_1 + 36d_3 + 52d_4 - 19d_{34} + 10\gamma_3$
	161	152.6	$15d_4 + 18\gamma_3 + 12\gamma_4 + 12\gamma_6 + 19\gamma + 16\alpha$ $(8\alpha_2)$
Eg	564	576.8	$11d_1 + 51d_2 + 9d_3 + 8d_{12}$
	429	453.6	$15d_3 + 47d_4 + 9\gamma_3 + 9\gamma_4 + 23\gamma$
	329	346.1	$52d_1 + 42d_3 + 12d_4 - 23d_{13} - 7d_{14}$
	193	171.6	$20d_1 + 22d_2 + 16d_3 + 25\gamma_4 + 11\alpha$
Fg	591	575.7	$22d_1 + 43d_2$
	564	546.3	$20d_1 + 34d_2 + 12d_3 + 7d_{13} + 12\gamma$
	526	530.5	$31d_1 + 37d_2$
	469	463.3	$19d_2 + 38d_4 + 26\gamma$
	429	438.9	$21d_1 + 40d_4 + 23\gamma$
	399	405.5	$15d_1 + 54d_4 - 13d_{14} + 31\gamma$
	376	379.7	$32d_1 + 42d_3 + 16d_4 - 15d_{13}$
	329	340.0	$40d_1 + 43d_3 - 25d_{13} + 26\gamma$
	318	319.3	$48d_1 + 44d_3 + 13d_4 - 26d_{13} - 15d_{34} + 22\gamma$
	193	209.7	$19d_2 + 26d_4 + 10\gamma_7 + 26\gamma + 10\alpha$
	179	189.9	$14d_1 + 23d_2 + 17d_3 + 7d_{13} + 20\gamma + 12\alpha$
	161	148.7	$23d_2 + 24d_3 + 9\gamma_1 + 9\gamma_2 + 12\gamma_4 + 9\gamma_6 + 9\alpha$
	129	117.4	$12d_3 + 12\gamma_3 + 11\gamma_4 + 11\gamma_5 + 11\gamma_6 + 11\gamma_7 + 11\gamma + 17\alpha$
	116	111.2	$10d_3 + 31\gamma_4 + 18\gamma_5 + 10\gamma_7 + 10\gamma + 16\alpha$
Fu	575	590.0	$21d_1 + 32d_2 + 7d_{12}$
	555	550.1	$28d_1 + 35d_2 + 9d_{12}$
	490	514.2	$17d_1 + 42d_2 + 12d_3 + 7d_{13}$
	462	459.2	$19d_2 + 45d_4 + 29\gamma$
	430	427.6	$9d_2 + 52d_4 + 26\gamma$
	415	404.8	$12d_1 + 10d_3 + 44d_4 + 8d_{34} + 21\gamma$
	372	368.9	$48d_1 + 47d_3 - 20d_{13} + 13\gamma$
	335	338.1	$61d_1 + 35d_3 - 30d_{13} + 25\gamma$
	302	330.7	$46d_1 + 34d_3 + 12d_4 - 25d_{13} - 8d_{14} - 15d_{34} + 9\gamma_2 + 11\gamma_4 + 19\gamma$
	242	237.8	$18d_1 + 30d_2 + 10d_3 + 10d_4 - 8d_{12}$
	183	198.6	$13d_1 + 21d_2 + 29d_3 + 11d_4 + 8d_{13} - 11d_{34} + 24\gamma$
	172	173.8	$9d_4 + 9\gamma_2 + 9\gamma_3 + 9\gamma_4 + 10\gamma_5 + 16\gamma_6 + 9\gamma_7 + 21\alpha$
	n.o.	166.9	$9d_3 + 18\gamma_1 + 9\gamma_2 + 12\gamma_5 + 8\gamma_6 + 13\gamma_7 + 17\alpha$
	n.o.	151.7	$11d_1 + 20d_2 + 31d_3 + 22d_4 - 11d_{12} - 13d_{34} + 10\gamma_5 + 19\gamma + 11\alpha$
	120	121.7	$42\gamma_1 + 11\gamma_4 + 9\gamma_5 + 12\gamma + 11\alpha$
	n.o.	107.0	$15\gamma_1 + 41\gamma_4 + 19\gamma + 12\alpha$

Note. n.o., Nonobserved.

of experimental spectra recorded at high pressures and high temperatures (18); therefore it seems quite valid.

Calculations also give the eigenvector matrix and consequently the normal modes of vibrations. From the normal modes, it was possible to justify our previous assignments: for example, the 591 cm^{-1} A_g and F_g modes and the 564 cm^{-1} E_g and F_g modes exhibit very close normal modes.

The stretching force constants of the four Y–O bonds are quite different. The d_1 ($Y_{(C_{3i})}$–O) bonds exhibit a stretching force constant of 1.20 N · cm^{-1}. The d_2, d_3, and d_4 bonds belonging to the $Y_{(C_2)}O_6$ octahedra exhibit stretching force constants of 1.25, 0.80 and 0.90 N · cm^{-1}, respectively, with an average value of 0.98 N · cm^{-1}. The $Y_{(C_{3i})}$–O bonds thus seem more rigid than the $Y_{(C_2)}$–O ones, in agreement with the results of Jollet *et al.* (19) who showed by XPS measurements that the $Y_{(C_{3i})}$–O bonds are slightly more covalent than the $Y_{(C_2)}$–O bonds.

On average the principal force constants are 1.03 N · cm^{-1} for the Y–O stretching, 0.44 N · cm^{-1} for the O–Y–O bending, and 0.20 N · cm^{-1} for the Y–O–Y bending. It is interesting to compare these values with those calculated for α-Al_2O_3, which were, respectively, 1.14, 0.47, and 0.24 N · cm^{-1} (20). In α-Al_2O_3 the coordination of atoms is the same as in Y_2O_3, but the linkage of the AlO_6 octahedra is made by corners and edges as in Y_2O_3 and also by faces, giving a very high compactness to the structure. It can be observed that

(i) the force fields are very close for the two compounds; the Al–O and Y–O bonds have a degree of covalence of the same order;

(ii) however, all the force constants are higher in Al_2O_3 than in Y_2O_3, particularly the Y–O–Y bending constants. It can be concluded that α-Al_2O_3 exhibits a more rigid structure than Y_2O_3.

CONCLUSION

In this work, we have measured precisely the vibrational spectra of the cubic form of Y_2O_3, especially by Raman polarized spectra and have proposed an assignment of the Raman and IR frequencies to the different modes of vibration. Then, a NCA allowed us to determine a complete GVFF. A comparison of the GVFF of Y_2O_3 and α-Al_2O_3, in which the atoms exhibit the same coordination, showed that the structure of α-Al_2O_3 is the more rigid.

ACKNOWLEDGMENTS

The authors are indebted to A. M. Lejus for providing a single crystal of Y_2O_3, to C. Dembinski for providing sintered samples, and to K. Rotereau for help in obtaining the Laue patterns. This work was supported by DRET.

REFERENCES

1. I. Warshaw and R. Roy, *J. Phys. Chem.* **65,** 2048 (1961).
2. L. Pauling and M. D. Sappel, *Z. Kristallogr.* **75,** 128 (1930).
3. M. G. Paton and E. N. Maslen, *Acta Crystallogr.* **19,** 317 (1965).
4. A. Fert, *Bull. Soc. Fr. Mineral. Cristallogr.* **89,** 194 (1966).
5. B. H. O'Connor and T. M. Valentine, *Acta Crystallogr. Sect. B* **25,** 2140 (1969).
6. W. L. Baun and N. T. McDevitt, *J. Am. Ceram. Soc.* **46,** 294 (1963).
7. N. T. McDevitt and A. D. Davidson, *J. Opt. Soc. Am.* **56,** 636 (1966).
8. Y. Nigara, *Jpn. J. Appl. Phys.* **7,** 404 (1968).
9. W. B. White and V. G. Keramidas, *Spectrochim. Acta Part A* **28,** 501 (1972).
10. G. Schaack and J. A. Koningstein, *J. Opt. Soc. Am.* **60,** 1110 (1970).
11. J. Gouteron, J. Zarembovitch, and A. M. Lejus, *C. R. Acad. Sci. Paris* **289,** C243 (1979).
12. A. M. Lejus and D. Michel, *Phys. Status Solidi B* **84,** K105 (1977).
13. J. H. Schachtschneider, "Shell Development Co. Technical Report 231-264," p. 57 1964.
14. J. B. Bates, *J. Chem. Phys.* **56,** 1910 (1972).
15. T. Shimanouchi, M. Tsubo, and T. Miyazawa, *J. Chem. Phys.* **35,** 1597 (1961).
16. S. Bhagavantam and T. Venkataryudu, *Proc. Indian Acad. Sci. A* **9,** 224 (1939).
17. D. Bloor and J. R. Dean, *J. Phys. C: Solid State Phys.* **5,** 1237 (1972).
18. Y. Repelin, C. Proust, E. Husson, and P. Gillet, *J. Phys. Chem. Solids,* to be published.
19. F. Jollet, C. Noguera, N. Thomson, N. Thromat, M. Gautier, and J. P. Durand, *Phys. Rev. B* **42,** 7587 (1990).
20. Y. Repelin, E. Husson, and C. Proust, *J. Solid State Chem.* **116,** 378 (1995).